**DE-FG02-06ER15795** **Dionisios (Dion) G. Vlachos (U. of Delaware)**

# *HYDROGEN INITIATIVE*: AN INTEGRATED APPROACH TOWARD RATIONAL NANOCATALYST DESIGN FOR HYDROGEN PRODUCTION

Department of Chemical Engineering
University of Delaware
Newark, DE 19716
Phone number: 302-831-2830; Fax number: 302-831-2048
*Email: vlachos@udel.edu*

Additional PIs: Douglas J. Buttrey and Jochen A. Lauterbach

Students: Elizabeth D'Addio, Hua Yang, Rohit Vijay
Postdocs: Ayman Karim, Vinay Prasad
Undergraduate students: Jason Binz and Anabel Pineiro

**Year one budget**: $337,678

**Period of execution**: July 1, 2006-June 30, 2009

**Starting date**: July 1, 2006

## Abstract

The overall objective of this grant is to develop a rational framework for the discovery of low cost, robust, and active nano-catalysts that will enable efficient hydrogen production. Our approach will be the first demonstration of integrated multiscale model, nano-catalyst synthesis, and nanoscale characterization assisted high throughput experimentation (HTE). We will initially demonstrate our approach with ammonia decomposition on noble metal catalysts. Our research focuses on many elements of the Hydrogen Initiative in the Focus Area of "Design of Catalysts at the Nanoscale'. It combines high-throughput screening methods with various nanostructure synthesis protocols, advanced measurements, novel *in situ and ex situ* characterization techniques, and multiscale theory, modeling and simulation. This project directly addresses several of the long-term goals of the DOE/BES program. In particular, new nanoscale catalytic materials will be synthesized, characterized and modeled for the production of hydrogen from ammonia and a computational framework will be developed for efficient extraction of information from experimental data and for rational design of catalysts whose impact goes well beyond the proposed hydrogen production project.

In the first year of the grant, we have carried out HTE screening using a 16 parallel microreactor coupled with an FTIR analysis system. We screened nearly twenty single metals and several bimetallic catalysts as a function of temperature, catalyst loading, inlet composition, and temperature (order of 400 experiments). We have found that Ru is the best single metal catalyst and no better catalysts were found among the library of bimetallics we have created so far. Furthermore, we have investigated promoting effects (i.e., K, Cs, and Ba) of the Ru catalyst. We have found that K is the dominant promoter of increased Ru activity. Response surface experimental design has led to substantial improvements of the Ru catalyst with promotion, especially at lower temperatures. It has been found that the promoting effect is not limited to K but extendible to some other alkaline metals. In addition, we have studied a number of synthesis variables, including the effects of support, solvent used, calcination temperature and time. It has been found that solvent and support could have an important effect on activity. Advanced characterization of the Ru/K promoted catalyst has been carried via SEM, TEM, selected-area electron diffraction, and energy dispersive x-ray spectroscopy.

It has been found that the Ru catalyst is composed of agglomerates, whereas the K-promoted catalyst of “nanowhiskers” with a $KRu_4O_8$ hollandite structure. Our detailed characterization studies strongly suggest for the first time a strong correlation between hollandite formation and the high activity of Ru catalyst. Future work should provide stronger evidence of this correlation and may enable us to further improve the catalyst. A number of microkinetic models for single metals have been developed and a methodology for linking models for bimetallic catalysts in a thermodynamically consistent manner has been implemented. This enables us for the first time to start exploring multi-site catalysts, using either mean-field or Monte Carlo approaches, and filling the materials gap from single crystals to supported catalysts. In addition, we are developing a multiscale model-based design of experiments methodology. This framework employs multiscale-based models combined with global search in experimental parameter space, identification of novel experimental conditions that maximize the kinetic information content, followed by statistical analysis that can guide the next iteration of experiments.

## Recent Progress

### A. High throughput screening

*Exploration of single metal and bimetallic catalysts for ammonia decomposition*

An array of single metals was tested to find potentially better candidates for $NH_3$ decomposition using a 16 parallel reactor system coupled with an FTIR analysis system. Some of these data have been used to develop microkinetic models, as elaborated below. These metals (along with the respective weight loadings on $Al_2O_3$) are: Pd (4%), Cs (10%), Mg (10%), V (10%), In (10%), Sn (10%), Ti (10%), Zn (10%), Rb (10%), Rh (10%), Fe (10%), Co (10%), Sr (10%), Ni (10%), K (12%), Ir(0.5-5%), Pt(0.5-5%), Ru(0.5-5%), and Ca (12%). Except for Ru, Rh, Fe, Pt, Ir, and Co, none of the other metals showed any significant activity. Among these catalysts, Ru is the best, consistent with literature studies focused mainly on ammonia synthesis. In addition, we have screened several bimetallics. In order to search for low cost catalysts, we have chosen to focus on bimetallics by adding various amounts of different metals to 5% (wt) Co. The additives included: Rh, Cs, Rb, Li, Ni, Fe, Zn, and Ba at fractions of 10, 100, 1000, and 10000 ppm.

In summary, we synthesized and tested more than 50 different catalyst combinations. Each catalyst was tested at 7 different temperatures (200ºC to 500ºC in steps of 50ºC), giving a total of more than 350 experiments. In addition, we performed $N_2$ and $H_2$ inhibition studies (i.e., adding 10% $N_2$ or $H_2$ to the feed stream (containing $NH_3$ and He) and studying its effect on the performance of that catalyst) for each one of those combinations. No better potential lead than Ru resulted from these initial exploratory studies.

*Promotion of Ru catalyst*

It has been found that Ru is the most active single metal for the synthesis as well as decomposition of $NH_3$ [1-5] and verified by our experiments reported above. In addition, it has also been reported that the alkali and alkaline earth metals, with emphasis on K, Cs and Ba, act as good promoters (for both synthesis and decomposition) increasing the $NH_3$ conversion efficiency at low temperatures [3, 6-14]. There have been various studies to identify the effect of support on the performance of these catalysts [3, 4, 15]. Recently, it has been proposed that Ru promoted with K supported on carbon nanotubes (CNTs) is a very efficient catalyst for $NH_3$ decomposition [3, 4]. Other studies have also reported an increase in $NH_3$ decomposition efficiency using $ZrO_2$ treated with KOH as a support material [16]. However, the information on the role of promoters and the mechanism of promotion is limited and inconsistent. It has been claimed that K and Cs act as promoters by allowing electrons to be transferred to the support,

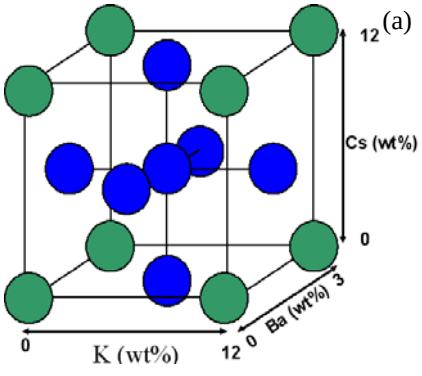


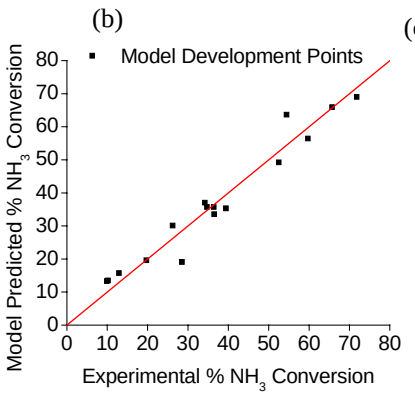


(c)

| Term | Coefficients |
|---|---|
| Constant | 35.7 |
| Ba | -1.8 |
| K | 22.3 |
| Cs | -2.6 |
| Ba*Ba | -0.5 |
| K*K | 5.6 |
| Cs*Cs | -3.0 |
| Ba*K | -0.9 |
| Ba*Cs | -1.0 |
| K*Cs | -4.7 |

**Figure 1.** a) Response Surface Model for Ba/Cs/K system with 4% Ru on Alumina Support. b) Model prediction compared to experimental data. c) List of the normalized model coefficients.

facilitating the desorption of $N_2$ off the surface of the catalyst (in the case of synthesis), whereas Ba has been suggested to disperse the metal over the support allowing increased surface area and presumably a higher turnover frequency [2, 7-9, 13]. Currently, no conclusive evidence exists to support these claims. Most of these studies are lacking comprehensive characterization of the catalyst.

We investigated the effect of adding different promoters upon a 4 (wt/wt %) Ru by varying weight percents of K (0-12 %), Cs (0-12 %), and Ba (0-3 %). The loading diagram is shown in Figure 1a. The catalysts were synthesized via incipient wetness on $\gamma$-$Al_2O_3$ support and ruthenium chloride, potassium nitrate, cesium chloride, and barium nitrate as precursors. The gas mixture used for catalyst testing was 10% $NH_3$ in He. The catalysts were tested by heating this mixture from 200 ºC to 500 ºC and by measuring the $NH_3$ conversion every 50 ºC.

In order to effectively determine the impact of each promoter, a response surface study was conducted for the Cs/Ba/K promoted system at a constant weight percent of Ru (4%). The design for the metal composition is shown in Figure 1. A quadratic response surface model was developed for the % $NH_3$ conversion at 350 ºC as a function of metal composition, given by Eq. 1. The total number of catalysts tested for this study was 17.

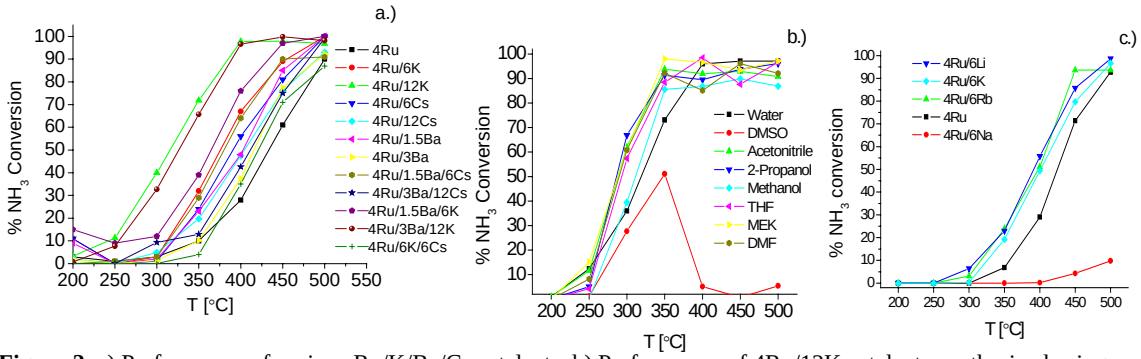


**Figure 2.** a) Performance of various Ru/K/Ba/Cs catalysts. b) Performance of 4Ru/12K catalysts synthesized using different solvents. c) Effect of adding other alkali metals as promoters to Ru catalyst.

$$R = C + \alpha_1(K) + \alpha_2(Cs) + \alpha_{12}(Ba)....+\beta_1(K)^2 + \beta_2(Cs)^2....+\lambda_1(K*Cs) + \lambda_2(K*Ba) \qquad (1)$$

It was found that addition of 12%K to 4 wt% Ru improves the $NH_3$ conversion efficiency at 350ºC by ~35%, as shown in Figure 2a. Figure 1b compares model predictions with the experimental data and Figure 1c lists the normalized model coefficients.

Based on the model coefficients, the promotional effect is attributed to K, whereas Ba and Cs have minimal effect. Similar trends can also be observed from the experimentally observed results shown in Figure 1. It is clear that K has a huge promotional effect on the $NH_3$ conversion at lower temperatures with 4Ru/12K outperforming all other combinations (Figure 2a). Another response surface study around Ru (2-8%) and K (0-18%) predicted that the optimum K composition occurs at even higher weight loadings (~5% Ru/18% K). This catalyst still needs to be synthesized, tested, and characterized to confirm model predictions. Figure 2c shows that both Li and Rb cause a similar promotional effect as K, but Na is not effective.

Based on TEM/SEM characterization of these catalysts (see below), it was identified that the 4Ru/12K catalyst is present in the form of a complex tubular structure assigned to $KRu_4O_8$. It has been earlier reported that such tubular structure is characteristic of a family of compounds called hollandites [17-25]. Due to their peculiar 1D tunnel like structure, hollandites have extensively been studied for use as 1D ionic conductors [18]. The suggested methods of synthesizing these compounds include use of an extremely high content of tunnel cations, in our case K, or high pressure [23]. It has also been reported that the synthesis of such hollandite structures is sensitive to the type of cations, their relative sizes, and also calcination temperature [17]. There is evidence

in the literature of $KRu_4O_8$ synthesis at 750°C using a Ru:K ratio of 1:8 (atomic ratio) [18]. In contrast to these studies, we use a Ru:K ratio of ~7.5 and much lower calcination temperatures (up to 550°C) to form similar structures. The promotional effect of 4Ru/12K can be attributed to either the increase in dispersion of Ru or to the electronic promotion of K, both of which can be related to the formation of $KRu_4O_8$ hollandite structure. Further work is needed to fully correlate synthesis conditions with the formation and stability of hollandite and the effect of the latter on the dispersion and activity of the Ru catalyst.

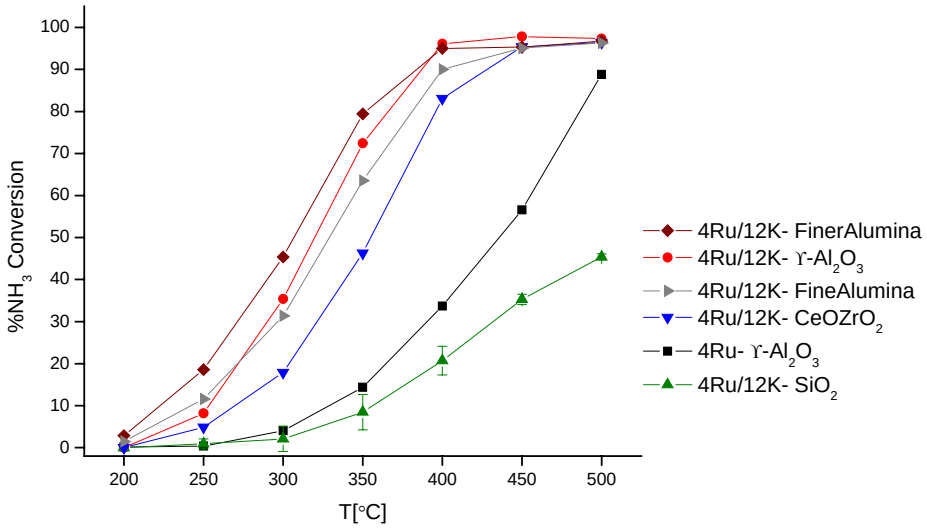


**Figure 3**. Performance of 4Ru/12K catalysts synthesized on a variety of supports.

Figure 3 shows the effect of different supports. It is clear that the support can have a large effect on activity. It is interesting to note that all the samples prepared on Alumina show better performance relative to others. The catalysts synthesized using different supports have not been characterized yet to comment on the role of hollandite in the observed promotional effect (work in progress).

Figure 2b shows the effect of solvent used in synthesis on catalyst activity. Figure 4 shows SEM pictures of the catalysts synthesized using different solvents. The distinctively different behavior of DMSO, in Figure 2b, can be attributed to the poisoning of the surface from S (also seen from the formation of big Ru boulders on the catalyst surface). It was also found that hollandite structures were present in each of the catalyst made using different solvents (except DMSO) and that could also explain the almost similar behavior of these catalysts.

Since hollandites are sensitive to the synthesis conditions, we have also investigated the effect of calcination time and temperature as well as the synthesis of Ru/Ba and Ru/Sr catalysts synthesized by heating up to 1100°C (data not shown). Overall, our results indicate that the different supports and/or solvents, catalyst calcination, and ammonia composition change the dispersion of Ru and the presence of hollandite may be essential for high catalyst activity. However, further characterization of select catalysts using CO chemisorption and microscopy is needed to identify the active surface area and further correlate synthetic protocols with the presence of hollandite and catalyst activity.

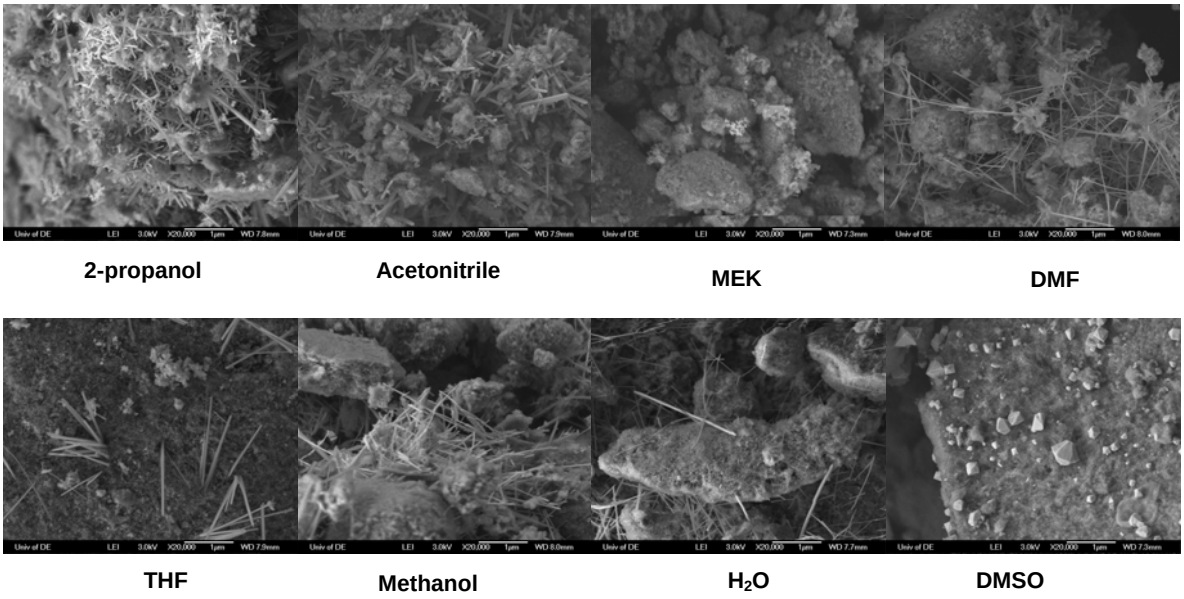


**Figure 4**. SEM analysis of 4Ru/12K catalyst prepared using different solvents.

## B. Advanced Characterization of Catalysts

Advanced characterization was focused on the K promoted catalysts synthesized using $H_2O$ since the 4Ru/12K showed enhanced performance over the Ru monometallic catalyst. Characterization was aid at identifying the differences between the active vs. less active catalyst. Figure 5a and 5b show representative post-calcination TEM and SEM images for the Ru catalyst and Figure 5c and 5d show images for the 4Ru/12K catalyst. The Ru catalyst is composed of agglomerates that range in size from 30 nm up to a micron. Ru agglomerates are well-distributed on the support, but the surface area is low due to the large particle

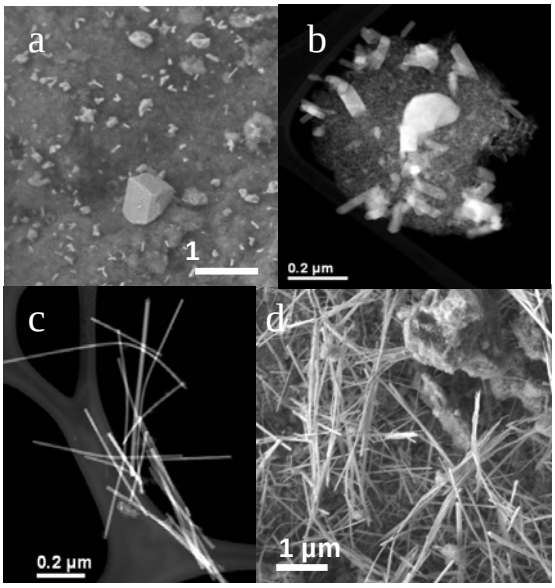


**Figure 5.** Representative TEM (b & c) and SEM (a & d) images showing the pure $Ru/Al_2O_3$ catalyst (a & b) and the K-promoted $Ru/Al_2O_3$ catalyst (c & d).

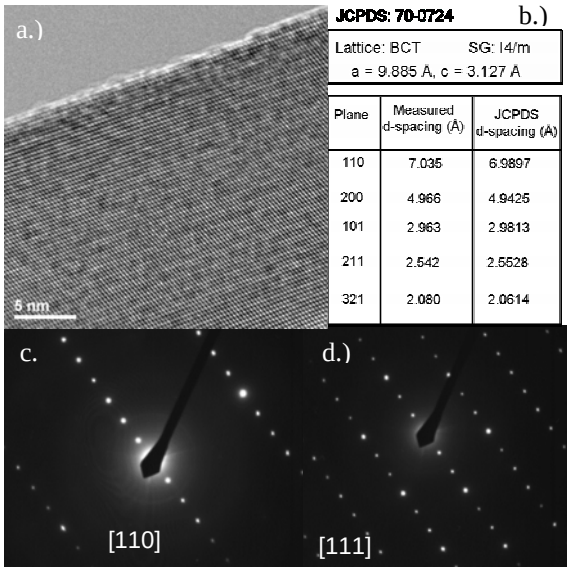


**Figure 6.** Post-calcination characterization of the "nanowhiskers" using (a) high resolution imaging, (c & d) selected-area electron diffraction. Table in (b) compares the experimental d-spacings to a known potassium Ru oxide.

size. In contrast, the K-promoted catalyst is composed of a complex network of "nanowhiskers" that cover the surface of the $\gamma$-$Al_2O_3$ support. The whiskers have a rectangular base that exhibits edge lengths of 10-50 nm and lengths that can extend from a few nm to several microns.

Further TEM characterization revealed that the whiskers are crystalline as evidenced by the high-resolution image showing the well-ordered atomic level structure. The whiskers have a $KRu_4O_8$ hollandite structure that was confirmed using individual "whiskers" and selected-area electron diffraction (SAED). Figure 6b shows the experimentally measured interplanar d-spacings compared to the known hollandite structure (JCPDS card 70-0724). Assuming the whiskers are the active phase, the possibility of an active hollandite structure is significant since this is one member of a large class of materials. Members of the hollandite class have the general formula $A_xB_4O_{16}$, where A is typically a large cation (Ba, K, Na, Sr, Rb), B a cation that can form oxygen octahedra (Mn, Ti, Al, Ru), and x is typically near one and controls the mix of +3 and +4 valence on the B-site. The identity of A and B can be mixed to form a large variety of materials. Characterization after reaction is shown in Figure 7. SEM shows four distinct structures. The first two have already been discussed and are the $Al_2O_3$ support material and the hollandite "nanowhiskers". The third structure in Figure 7a (boxed) appears to be nanoparticles and nanowires with an irregular morphology (also shown in the TEM in 7b). These nanowires were probed further using energy dispersive x-ray spectroscopy (EDS) in Figure 7d (blue line). The assignment of the peaks indicates that these nanowires are Ru metal. The large C peak is due to the supportive film of the Cu grids used for the TEM analysis. Ru wires were only observed in the post-reacted sample and were assumed to form during the reaction. The fourth structure shown in 7c is glassy-like in appearance. EDS (black line) shows the elements K, Cl, Al, and O. The Al and O can be attributed to the support and the K and Cl appear to form a KCl structure.

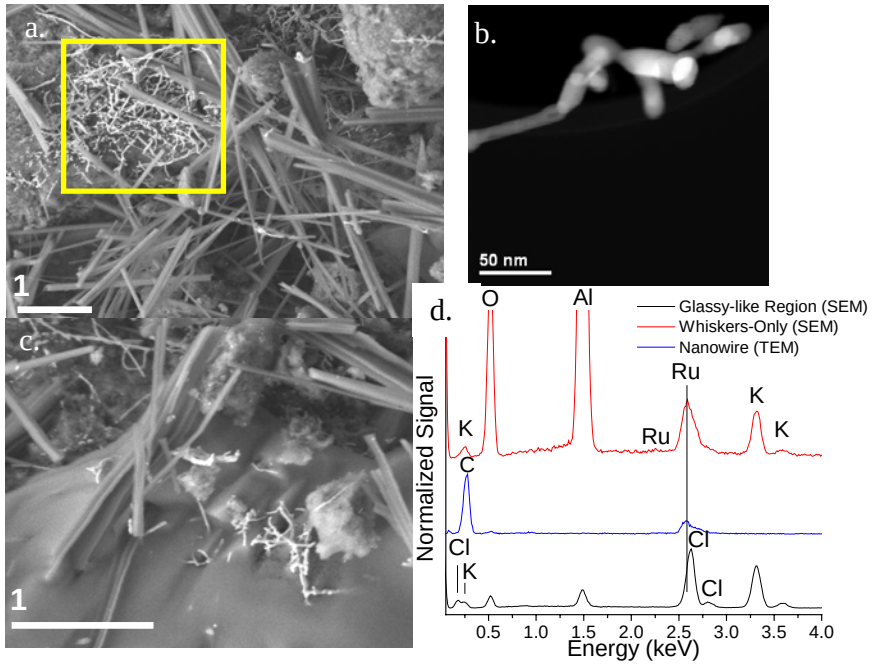


**Figure 7.** Representative SEM (a & c) and TEM (b) images of the K-promoted $Ru/Al_2O_3$ after $NH_3$ decomposition. Elemental analysis using energy dispersive x-ray spectroscopy is shown in (d).

### C. Multiscale Modeling Toward Development of Better $NH_3$ Decomposition Catalysts

*Development of a library of microkinetic models*

Our group employs a hierarchical multiscale methodology for microkinetic model development. We start with semi-empirical methods, such as the Unity Bond Index-Quadratic Exponential Potential (UBI-QEP) theory, known also as bond-order conservation (BOC), and crude transition state theory (TST), for parameter estimation. Major advantages of our semi-empirical approach include its computational speed and the fact that it is amenable to

experimental and/or density functional theory (DFT) input and refinement. As a result, it can indirectly take into account polycrystallinity and/or support effects and the often important adsorbate-adsorbate interactions, by a suitable choice and parameterization of heats of chemisorption, to close the materials and pressure gaps. As one example, the bond index of UBI-QEP can be adjusted based on the picture emerging from DFT calculations about homologous series having a similar transition state (early or late, etc.). Furthermore, DFT estimated adsorbate-adsorbate interactions, which are nearly impossible to obtain experimentally for intermediates, can easily be mapped into the UBI-QEP method to substantially improve model predictions.

Using this methodology (semi-empirical methods plus refinement using a limited number of DFT calculations and thermodynamic consistency) and HTE data, we developed microkinetic models for various catalysts. An example is shown in Figure 8. We have found significant difference in dominant adsorbates and also in the effect of lateral interactions on the chemistry among various catalysts studied. This finding has important implications for catalyst design; it indicates that it may not correct to simply study a single elementary reaction step via DFT for identifying better catalysts, at least for some processes. This approach is being extended to a library of catalysts. In addition, a framework for linking models for different catalysts in a thermodynamically consistent manner has been developed. One application of this framework is to predict the activity of heterogeneous catalysts consisting of multiple types of sites, including various crystallographic planes, edges, and corners in nanoparticles of Ru catalyst. This framework is suitable for either mean-field or Monte Carlo models, and we currently explore both types of models.

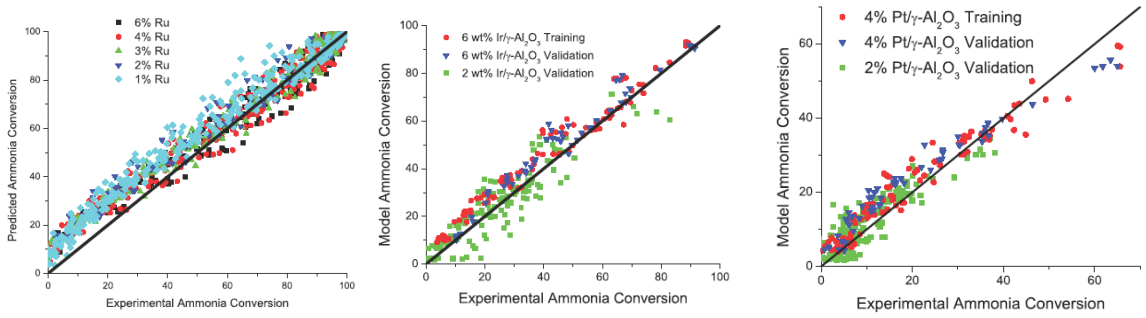


**Figure 8**. Parity graphs of HTE and model prediction for $NH_3$ conversion for Ru (left), Ir (middle), and Pt (right). For the Ru catalyst, more than 1000 experimental points have been collected and simulated.

*Model-based design of experiments for assessing model accuracy and designing better catalysts*

Models are typically developed using a rather limited set of experimental data. As a result, the model reliability for prediction outside their range of fit is always questionable. This aspect severely undercuts the use of a model in optimization of reactors and in search for better catalysts. Despite the power of HTE, screening the experimental variable space (of 7 variables) for a system as simple as $NH_3$ with 5-6 experiments in each variable (and all possible combinations) requires of the order of 100,000 experiments. This is beyond the scope of most massive HTE systems available. It is therefore important to develop a framework that can suggest a handful of experiments that are sufficiently novel to test experimentally. With this goal in mind, we are developing a new framework for multiscale model-based design of experiments.

Once a microkinetic model has been developed using the multiscale methodology outlined above and HTE data, the framework is run to predict novel experimental combinations. These experiments are then conducted and their results compared to model predictions in some observable (e.g., ammonia conversion, most abundant reactive intermediate, etc.). The model is

refined if necessary with respect to its parameters and/or its structure. The entire procedure is repeated until the deviation between model and experiments in the entire experimental parameter space is low.

The computational methodology involves various tools, such as identifiability and sensitivity analysis, principal component analysis (PCA) and clustering methods. The procedure can be outlined as follows: thousands of sets of operating conditions are randomly generated, and sensitivity analysis is performed with respect to the kinetic parameters of a microkinetic model. Normalized sensitivities of the ammonia conversion and fractional coverage of surface species (H, N and vacant Ru sites, which are the dominant surface species predicted by the model) are calculated, and operating conditions that maximize these sensitivities are recorded. k-means clustering is performed on these data sets to find common features among their members and to suggest experiments to be performed at the centroids of the identified clusters. We have used either 2 or 3 clusters on the data sets whose sensitivities are above a threshold value. Finally, identifiability analysis is carried out to ensure that these kinetic parameters can indeed be determined from experimental data. This involves calculating the Fisher information matrix (FIM) from the matrix of sensitivities. The FIM indicates that only the forward pre-exponential factors are identifiable (due to thermodynamic constraints). An eigenvalue-eigenvector analysis of the FIM indicates that the pre-exponential for the $N_2$ dissociation reaction is not independently identifiable in our model.

Figures 9 and 10 show typical results from clustering analysis on Ru catalyst identifying inlet composition and other experimental conditions that maximize model information with respect to $H_2$ dissociation/association. Similar graphs have been generated for all kinetic parameters. These experiments can be summarized by plotting the centroids of all clusters for all elementary reaction steps of the mechanism (Figure 11). Note that only a handful of experiments are needed to verify the model (instead of thousands needed when one parameter at a time is varied). In addition, novelty sampling can be used to pick up combinations of experimental variables that are most diverse within a cluster. Using this information, we are in the process of carrying out experiments to validate model predictions and/or improve models. This will be repeated for the entire library of microkinetic models. This library will subsequently be used for catalyst design.

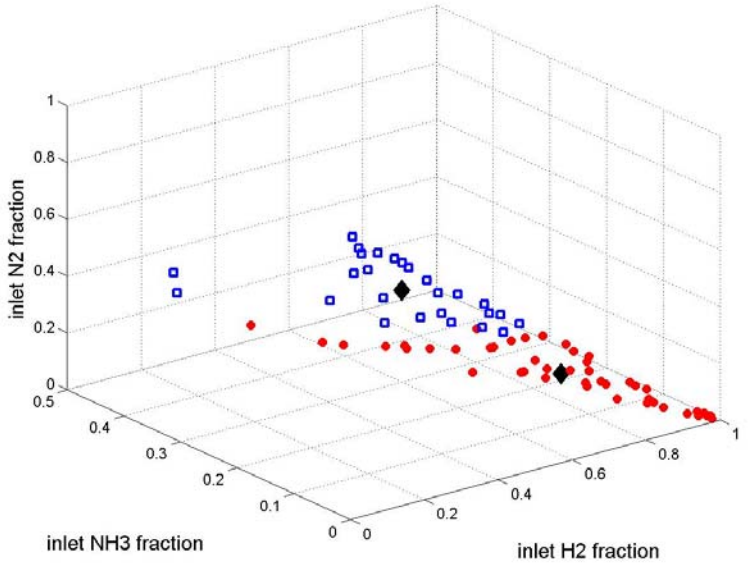


**Figure 9.** Clustering analysis for high sensitivity with respect to $H_2$ dissociation reaction step. Filled red circles show the inlet gas mass fractions for the first cluster, and blue squares show the fractions for the second cluster. Black diamonds show the centroids of the clusters.

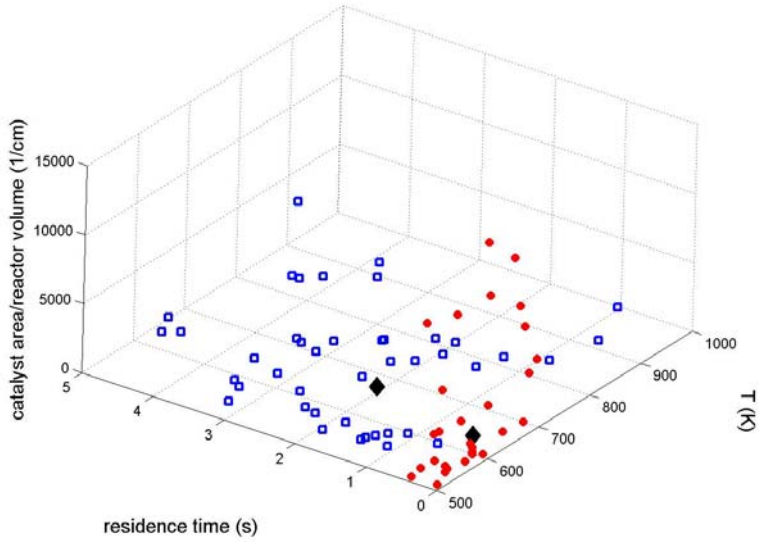


**Figure 10**. Clustering analysis for high sensitivity with respect to $H_2$ dissociation. Variables shown are temperature, residence time and area of catalyst per unit reactor volume, corresponding to Figure 9.

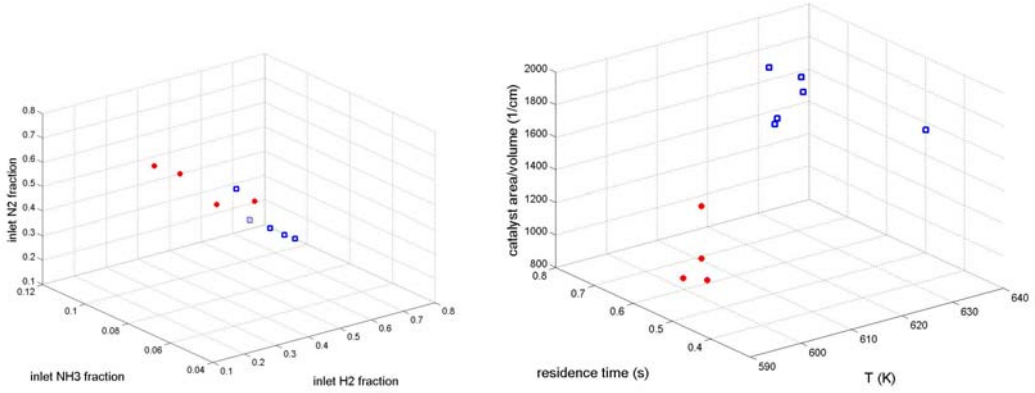


**Figure 11**. Summary of centroids of clusters of high sensitivity with respect to each of the elementary steps in the $NH_3$ mechanism on Ru. Red circles indicate the first cluster and blue squares the second. Variables shown are inlet gas mass fractions (left) and temperature, residence time and area of catalyst per unit reactor volume (right). Note that only a handful of experiments are needed to test the model.

## Objectives for Next Year

We plan to continue on with the objectives listed in the proposal. Given the findings from the first year, we anticipate the following studies: Further characterize various catalysts with different promoters and synthetic protocols to identify the mechanism of promotion and the effect of solvents and supports on the formation and stability of hollandites and on catalyst activity; Use this information to identify optimal conditions that lead to the formation of hollandite structures and could aid in further enhancing the performance of the existing catalysts; Complete a fairly rich library of microkinetic models on single metals for rational selection of bimetallic catalysts; Test microkinetic models against experimental data predicted via the multiscale-model based design of experiments approach and refine models as needed; Confirm important findings via DFT; Use these models to identify better multicomponent catalysts to synthesize for our future experimental studies.

## Publications and Presentations Fully Supported from this Grant

1. V. Prasad, A. Karim, N. S. Kaisare, D. Hansgen, and D. G. Vlachos, "A unified modeling framework for design of multi-site catalysts: Application to $NH_3$ decomposition for $H_2$ production", 20th North American Catalysis Society Meeting, Houston, June 17-22, 2007 and in 81st ACS Colloid & Surface Science Symposium, Newark, DE, June 24-27, 2007.
2. W. Pyrz, R. Vijay, D. J. Buttrey, D. G. Vlachos, and J. Lauterbach, "Characterization of K-Promoted Ru Catalysts for Ammonia Decomposition Discovered Using High-Throughput Experimentation", in 20th North American Catalysis Society Meeting, Houston, June 17-22, 2007, in 81st ACS Colloid & Surface Science Symposium, Newark, DE, June 24-27, 2007, and in Catalysis Club of Philadelphia, March 2007, Newark, DE, as Poster Presentation.
3. V. Prasad, A. Karim, and D. G. Vlachos, "Multiscale model-based design of experiments using novelty sampling', AIChE J. (in preparation).
4. W. Pyrz, R. Vijay, D. J. Buttrey, and J. Lauterbach, "Characterization of K-Promoted Ru Catalysts for Ammonia Decomposition Discovered Using High-Throughput Experimentation", J. Cat. (in preparation).

## Statement of Unspent Funds for the Past Year

We have hired three graduate students and two postdocs (part time) to work on this project, in agreement with our annual budget. We do not expect substantial deviations from our approved budget.

## Update on Pending and Current Support

No other proposal is currently pending or funded related to this grant.

**Literature Cited**


[1] TV Choudhary, C Sivadinarayana, and DW Goodman, Catalytic ammonia decomposition: COx-free hydrogen production for fuel cell applications, *Catalysis Letters*, 72 (2001) 197.

[2] K-i Aika, T Takano, and S Murata, Preparation and characterization of chlorine-free ruthenium catalysts and the promoter effect in ammonia synthesis : 3. A magnesia-supported ruthenium catalyst, *Journal of Catalysis*, 136 (1992) 126.

[3] SF Yin, BQ Xu, XP Zhou, and CT Au, A mini-review on ammonia decomposition catalysts for on-site generation of hydrogen for fuel cell applications, *Applied Catalysis A: General*, 277 (2004) 1.

[4] SF Yin, QH Zhang, BQ Xu, WX Zhu, CF Ng, and CT Au, Investigation on the catalysis of COx-free hydrogen generation from ammonia, *Journal of Catalysis*, 224 (2004) 384.

[5] JC Ganley, FS Thomas, EG Seebauer, and RI Masel, A Priori Catalytic Activity Correlations: The Difficult Case of Hydrogen Production from Ammonia, *Catalysis Letters*, 96 (2004) 117.

[6] SJ Wang, SF Yin, L Li, BQ Xu, CF Ng, and CT Au, Investigation on modification of Ru/CNTs catalyst for the generation of COx-free hydrogen from ammonia, *Applied Catalysis B: Environmental*, 52 (2004) 287.

[7] RZ Sørensen, LJE Nielsen, S Jensen, O Hansen, T Johannessen, U Quaade, and CH Christensen, Catalytic ammonia decomposition: miniaturized production of COx-free hydrogen for fuel cells, *catalysis Communications*, 6 (2005) 229.

[8] W Raróg-Pilecka, D Szmigiel, Z Kowalczyk, S Jodzis, and J Zielinski, Ammonia decomposition over the carbon-based ruthenium catalyst promoted with barium or cesium, *Journal of Catalysis*, 218 (2003) 465.

[9] S Murata, and K-I Aika, Preparation and characterization of chlorine-free ruthenium catalysts and the promoter effect in ammonia synthesis. : 1. An alumina-supported ruthenium catalyst, *Journal of Catalysis*, 136 (1992) 110.

[10] S Murata, and K-i Aika, Preparation and characterization of chlorine-free ruthenium catalysts and the promoter effect in ammonia synthesis : 2. A lanthanide oxide-promoted Ru/Al2O3 catalyst, *Journal of Catalysis*, 136 (1992) 118.

[11] Z Kowalczyk, S Jodzis, W Raróg, J Zieliski, and J Pielaszek, Effect of potassium and barium on the stability of a carbon-supported ruthenium catalyst for the synthesis of ammonia, *Applied Catalysis A: General*, 173 (1998) 153.
[12] Z Kowalczyk, J Sentek, S Jodzis, E Mizera, J Góralski, T Paryjczak, and R Diduszko, An alkali-promoted ruthenium catalyst for the synthesis of ammonia, supported on thermally modified active carbon, *Catalysis Letters*, 45 (1997) 65.
[13] M Guraya, S Sprenger, W Rarog-Pilecka, D Szmigiel, Z Kowalczyk, and M Muhler, The effect of promoters on the electronic structure of ruthenium catalysts supported on carbon, *Applied Surface Science*, 238 (2004) 77.
[14] L Forni, D Molinari, I Rossetti, and N Pernicone, Carbon-supported promoted Ru catalyst for ammonia synthesis, *Applied Catalysis A: General*, 185 (1999) 269.
[15] SF Yin, BQ Xu, SJ Wang, CF Ng, and CT Au, Magnesia–Carbon Nanotubes (MgO–CNTs) Nanocomposite: Novel Support of Ru Catalyst for the Generation of COx-Free Hydrogen from Ammonia, *Catalysis Letters*, 96 (2004) 113.
[16] SF Yin, BQ Xu, SJ Wang, CF Ng, and CT Au, Nanosized Ru on high-surface-area superbasic ZrO2-KOH for efficient generation of hydrogen via ammonia decomposition, *Applied Catalysis A: General*, 301 (2006) 202.
[17] ML Carter, Tetragonal to monoclinic phase transformation at room temperature in $Ba_xFe_{2x}Ti_{8-2x}O_{16}$ hollandite due to increased Ba occupancy, *Materials Research Bulletin*, 39 (2004) 1075.
[18] ML Foo, W-L Lee, T Siegrist, G Lawes, AP Ramirez, NP Ong, and RJ Cava, Electronic characterization of alkali ruthenium hollandites: $KRu_4O_8$, $RbRu_4O_8$ and $Cs_{0.8}Li_{0.2}Ru_4O_8$, *Materials Research Bulletin*, 39 (2004) 1663.
[19] M Isobe, S Koishi, and Y Ueda, Ti-doping effect on the MI transition of hollandite vanadate, $K_2V_8O_{16}$, *Journal of Magnetism and Magnetic Materials*, 310 (2007) 888.
[20] T Klimczuk, W-L Lee, HW Zandbergen, and RJ Cava, Synthesis and magnetic properties of $(Ba,Bi)_{1.54}Rh_8O_{16}$ hollandite, *Materials Research Bulletin*, 39 (2004) 1671.
[21] ZQ Mao, T He, MM Rosario, KD Nelson, D Okuno, B Ueland, IG Deac, P Schiffer, Y Liu, and RJ Cava, Quantum Phase Transition in Quasi-One-Dimensional $BaRu_6O_{12}$, *Physical Review Letters*, 90 (2003) 186601.
[22] KN Marimuthu, and UV Varadaraju, Solid state studies on $Bi_{1.7-x}Hg_xV_8O_{16}$ (x = 0.4) and magnetic properties of alkali metal inserted $A_xBi_{1.7}V_8O_{16}$ (A = Li and Na) hollandite type phases, *Materials Chemistry and Physics*, 96 (2006) 22.
[23] O Tamada, N Yamamoto, T Mori, and T Endo, The Crystal Structure of K2Cr8O16: The Hollandite-Type Full Cationic Occupation in a Tunnel, *Journal of Solid State Chemistry*, 126 (1996) 1.
[24] T Waki, Y Morimoto, H Kato, M Kato, and K Yoshimura, Physical properties of $Ba_{1.09}V_8O_{16}$ with hollandite structure, *Physica B: Condensed Matter*, 329-333 (2003) 938.
[25] LC Nistor, GV Tendeloo, and S Amelinckx, Defects and Phase Transition in Monoclinic Natural Hollandite: $Ba_xMn_8O_{16}$, *Journal of Solid State Chemistry*, 109 (1994) 152.